Investigation of the role of Mg and Ca in the structure and durability of aluminoborosilicate glass

BACKHOUSE, Daniel, CORKHILL, CL, HYATT, NC and HAND, RJ

Investigation of the role of Mg and Ca in the structure and durability of aluminoborosilicate glass

D.J. Backhouse[1,*], C.L. Corkhill[1], N.C. Hyatt[1] and R.J. Hand[1,†]

[1]NucleUS Immobilisation Science Laboratory, Department of Materials Science and Engineering, University of Sheffield, Sir Robert Hadfield Building, Mappin Street, Sheffield, S1 3JD, UK

[†]corresponding author

Email: r.hand@sheffield.ac.uk

Tel: +44 (0)114 222 5465

Abstract

[*] Now at Sheffield Hallam University: Materials and Engineering Research Institute, Faculty of Science, Technology and Arts, City Campus, Howard Street, Sheffield, S1 1WB, UK

The structure and dissolution behaviour of $Na_2O{\cdot}CaO{\cdot}(15–x)Al_2O_3{\cdot}xB_2O_3{\cdot}SiO_2$ and $Na_2O{\cdot}MgO{\cdot}(15–x)Al_2O_3{\cdot}xB_2O_3{\cdot}SiO_2$ glasses, relevant to compositions of UK nuclear waste glass, have been investigated using nuclear magnetic resonance (NMR) spectroscopy and static dissolution experiments using the PCT protocol. Structural data from ^{11}B, ^{27}Al and ^{29}Si NMR analyses show that increasing the Increasing the $[B_2O_3]/([Al_2O_3]+[B_2O_3])$ ratio of the alkali-alkaline-earth aluminoborosilicate glasses led to an overall decrease in the proportion of non-silicate tetrahedral species (^{IV}Al + ^{IV}B) and a decrease in Si – O – X bonds (X = B, Al). The Mg-containing glasses exhibited lower ^{IV}B fractions than their Ca-containing counterparts, which is thought to be due to the presence of ^{IV}Mg tetrahedra in the network. The measured corrosion rates were similar for both Ca and Mg-containing glasses although unexpectedly some Ca-containing glasses exhibited higher corrosion losses than the Mg-containing ones for time periods up to 112 d. However, there was evidence of a greater tendency to rate resumption in the Mg containing than the Ca containing ones. Alteration products were found to contain Ca, Si and Al with the Ca containing glasses and Ca, Mg, Si and Al with the Mg containing glasses; Na was not detected in the alteration products although its presence cannot be ruled out based on the data obtained.

Keywords

Chemical durability, aluminoborosilicates, high pH environments

1. Introduction

In the United Kingdom, high level waste (HLW) arising from reprocessing of Magnox and oxide fuels is immobilised within a mixed-alkali borosilicate glass. Owing to the presence of a small amount of Magnox (Mg-Al alloy) cladding incorporated in reprocessing operations, the final vitrified product contains elevated concentrations of Mg (5.6 wt.% MgO [1]), compared with other international waste glasses arising from non-Magnox fuels (e.g. the French R7T7). The vitrification of other UK wastes with high Mg contents, such as Magnox sludge, is also being considered [2].

Since the internationally accepted solution for the disposal of long-lived radioactive wastes, including vitrified high level waste, is for isolation within a deep geological disposal facility, understanding the durability of these wasteforms in the presence of groundwater is essential. Magnesium, and calcium which is also present in UK HLW glass compositions, particularly those developed for post-operational clean-out operations [3], are known to play important roles in the glass dissolution process. For example, the presence of Mg in aluminoborosilicate glasses is known to accelerate the glass dissolution rate [4,5,6,7], however the mechanism that underpins this observation has not been elucidated. Calcium has been shown to play a critical role in the formation of calcium silicate hydrate (CSH) alteration layers on the glass surface during durability testing [8,9].

The geological disposal facility will utilise layers of containment to mitigate the release of radionuclides from the waste and subsequent transport to the biosphere. In the co-location scenario for an HLW and intermediate level waste repository currently under consideration for a UK geological disposal facility in hard rock [10], and for the Belgian super-container concept, a high pH cement will be used within the containment [11]. When groundwater contacts this material, it will buffer the groundwater to a pH between 10 and 13, and the chemistry will be dominated by $Ca(OH)_2$. Previous studies [9,12,13,14,15] have shown that the dissolution rate of silicate and borosilicate glasses increases as the pH becomes more alkaline, although the presence of Ca has been found to reduce the dissolution rate of some glasses when compared with dissolution in water, including the UK Mg-bearing nuclear waste glass, MW25 [9,16,17].

In this study, we present the results of an investigation aimed at understanding: (i) the influence of glass composition, particularly Mg or Ca content, and the B/Al ratio on glass structure and dissolution rate; and (ii) the effect of imposing Ca-rich, high pH conditions during the dissolution of aluminoborosilicate glasses on the mechanism of dissolution. The focus is on the structural

characterisation and dissolution of two glass series: $Na_2O{\cdot}CaO{\cdot}(15–x)Al_2O_3{\cdot}xB_2O_3{\cdot}SiO_2$ and $Na_2O{\cdot}MgO{\cdot}(15–x)Al_2O_3{\cdot}xB_2O_3{\cdot}SiO_2$.

2. Materials and methods

2.1 Glass synthesis and characterisation

Two series of aluminoborosilicate glasses were synthesised with nominal compositions (mol%) of $10Na_2O{\cdot}10CaO{\cdot}(15–x)Al_2O_3{\cdot}xB_2O_3{\cdot}65SiO_2$ (identified as $CA_{15-x}B_x$ throughout), and $10Na_2O{\cdot}10MgO{\cdot}(15–x)Al_2O_3{\cdot}xB_2O_3{\cdot}65SiO_2$ (identified as $MA_{15-x}B_x$ throughout), where x = 0, 5, 10 or 15 mol. %. Table 1 lists the batched compositions of the 8 glasses investigated.

Table 1. Batched and analysed (ICP-AES) compositions in mol% and details of the processing conditions for the 8 glasses investigated.

As batched (analysed) /mol%	Glass composition							
	$CA_{15}B_0$	**$CA_{10}B_5$**	**CA_5B_{10}**	**CA_0B_{15}**	**$MA_{15}B_0$**	**$MA_{10}B_5$**	**MA_5B_{10}**	**MA_0B_{15}**
Na_2O	10 (10.93)	10 (11.01)	10 (10.81)	10 (10.35)	10 (11.36)	10 (11.01)	10 (9.92)	10 (10.40)
CaO	10 (10.11)	10 (5.31)	10 (11.04)	10 (10.59)	0 (0.31)	0 (0.18)	0 (0.14)	0 (0.14)
MgO	0 (0.22)	0 (0.18)	0 (0.08)	0 (0.09)	10 (9.13)	10 (9.21)	10 (8.91)	10 (11.35)
Al_2O_3	15 (14.63)	10 (11.37)	5 (4.58)	0 (0.00)	15 (13.89)	10 (11.25)	5 (9.45)	0 (0.00)
B_2O_3	0 (0.00)	5 (5.31)	10 (11.37)	15 (16.28)	0 (0.00)	5 (5.59)	10 (9.82)	15 (16.38)
SiO_2	65 (64.11)	65 (67.11)	65 (62.13)	65 (62.68)	65 (65.30)	65 (62.76)	65 (61.76)	65 (61.73)
Total	100 (100)	100 (100)	100 (100)	100 (100)	100 (100)	100 (100)	100 (100)	100 (100)
Crucible type	Al_2O_3	Al_2O_3	Pt	Pt	Al_2O_3	Al_2O_3	Al_2O_3	Pt
Furnace	Gas	Gas	Electric	Electric	Gas	Gas	Gas	Electric
Melting temperature /°C	1550	1550	1450	1400	1550	1550	1550	1300
Melt duration /h	4	5	5	5	4	4	4	5
Stirred	No	No	Yes	Yes	No	No	No	Yes

The glasses were batched by mixing appropriate amounts of $NaHCO_3$ (Sigma-Aldrich 99.9%), $CaCO_3$ (Sigma-Aldrich 99.9%), $4MgCO_3.Mg(OH)_2.5H_2O$ (Sigma-Aldrich 99%), $Al(OH)_3$, (Sigma-Aldrich 99.9%), H_3BO_3 (Sigma-Aldrich 99.9%) and SiO_2 (Loch Aline sand). After mixing, as much of each batch as would fit was placed in an alumina crucible or a platinum crucible as indicated in Table 1. For

compositions melted in alumina crucibles the filled crucible was heated to 1100 °C in an electric furnace, before being transferred to a gas furnace, also at 1100 °C. The remaining batch was then transferred into the crucible and the crucible heated to 1550 °C at a heating rate of 10 °C min^{-1} and held at that temperature for 4 h. Glass frit was produced by pouring the melt through a steel mesh into water. For the compositions melted in a platinum crucible the filled crucible was placed in an electric furnace at 1450 °C or 1300 °C depending on composition (see Table 1); the remaining batch was added to the crucible after initial melt had been formed. After all the batch had been added and a batch free melt formed, it was stirred with a platinum paddle for 4 hours. A frit was produced in the same way as for the glasses melted in alumina crucibles. Initially it was thought that the higher temperature gas furnace would be required to make all of these glass compositions. During the manufacture of the initial glasses (the gas furnace used accommodates multiple crucibles) it was realised that this was not the case. Hence subsequent compositions were prepared using the electric furnace where a Pt crucible, instead of refractory crucibles that were more likely to dissolve into the melt, could be used. The composition of each glass was measured, following acid (HF) digest, by Inductively Coupled Plasma Atomic Emission Spectroscopy (ICP-AES, Spectros Ciros Vision). Comparison of the batched and measured compositions of the glasses indicates some deviations, however, overall the compositions were deemed to be acceptable to undertake subsequent work. Powders were produced using a Tema T100 Disc Mill. The density (Table 2) was measured using a helium pycnometer (Micromeritics Accupyc II 1340).

2.2 MAS-NMR Spectroscopy

Magic-Angle Spinning Nuclear Magnetic Resonance (MAS-NMR) spectroscopy (^{11}B, ^{27}Al and ^{29}Si) was performed on approximately 0.5 g of powder (< 75 µm) for each glass. NMR spectra were obtained at the EPSRC UK National Solid-state NMR Service at Durham University using a Varian VNMRS, operating at 128.301 MHz for ^{11}B, 104.199 MHz for ^{27}Al and 79.438 MHz for ^{29}Si. ^{11}B and ^{27}Al spectra were collected with a 4 mm (rotor outer diameter) probe, while the ^{29}Si spectra were collected using a 6 mm probe. Spinning rates were 11 kHz for ^{11}B and ^{27}Al, and 6 kHz for ^{29}Si. All spectra were acquired using a pulse-acquire experiment. Recycle delays were 5 s for ^{11}B, 0.2 s for ^{27}Al and 120 s for ^{29}Si. The ^{11}B, ^{27}Al and ^{29}Si spectra were referenced to BF_3/OEt_2, 1M aq. $Al(NO_3)_3$ and neat tetramethylsilane (TMS), respectively. The ^{11}B multiple-quantum (MQ) MAS-NMR experiment was carried out on the Varian VNMRS operating at 128.295 MHz with a 4 mm probe spinning at 12 kHz. The data were referenced to BF_3/OEt_2. The ^{27}Al triple-quantum (3Q) MAS-NMR experiment was carried out on a Bruker Avance III HD operating at 140 MHz, with a 1.9 mm probe spinning at 15 kHz, with frequencies referenced to 1M aq. $Al(NO_3)_3$.

2.3 PCT-B Dissolution Experiments

The dissolution of these glasses was assessed using the widely used accelerated powder based Product Consistency Test B (PCT-B) [18]. Equivalent monolith tests would have had to be run for much longer time periods. The Product Consistency Test B (PCT-B) protocol was followed for all dissolution experiments. Experiments were performed in a CO_2-free positive pressure N_2 glovebox to prevent carbonation of the dissolution medium, which was saturated $Ca(OH)_2$, produced by adding an excess of $Ca(OH)_2$ powder (> 0.92 g L^{-1}) to 400 mL of de-aerated ultra-high quality (UHQ) water (18.2 MΩ) water in a 500 mL HDPE vessel. The vessel was shaken vigorously to achieve full dissolution of $Ca(OH)_2$, and allowed to sit for several hours for the excess $Ca(OH)_2$ to settle at the bottom of the vessel. Solution preparation was also performed under CO_2-free conditions. An Advantec USY-1 ultrafilter unit filled with a slurry of $Ca(OH)_2$ powder and UHQ water was added to the vessel to maintain the pH of the leachant for the duration of the dissolution experiment. The 75 – 150 μm powder size fraction was used in the experiments and the powder surface area to solution volume (SA/*V*) ratio was 1200 ± 60 m^{-1}. This differs from the PCT standard (~2000 m^{-1}), due to the mass of glass available for the experiments, and also to maintain consistency with previous work on dissolution under high pH conditions [9]. The test vessels were placed in an LT Scientific OP39-UF oven within the glovebox, at 50 ± 2 °C. For each glass composition, duplicate experiments were performed; duplicate blanks were also tested.

5 ml aliquots of the leachate were taken after 1, 3, 7, 14, 28, 56 and 112 days. The elemental concentrations in the aliquots were determined by ICP-OES (iCAPduo6300, Thermofisher). The normalised mass loss, NL_i, in g m^{-2} of each element, *i*, was calculated using:

$$\mathrm{NL}(i) = \frac{C_i - C_{i_b}}{f_i\left(\mathrm{SA}/V\right)} \quad (1)$$

where C_i is the average concentration of *i* in solution in the duplicate experiments and C_{i_b} is the average concentration of *i* in the blank tests (both in g m^{-3}); f_i is the mass fraction of *i* in the glass monolith (unitless); SA is the surface area of the glass powder (in m^2); and *V* is the volume of solution (in m^3).

Glass powder samples were analysed, before and after dissolution, using a Bruker D2 Phaser diffractometer, with Cu$K_{\alpha 1}$ radiation (λ = 1.54056 Å), over an angular range of 10 – 65 °2θ, with a working voltage of 30 kV. Glass powders were also inspected following dissolution by scanning electron microscopy (SEM) coupled with energy dispersive spectroscopy (EDS), using a Hitachi

TM3030 and Bruker Quantax EDS to identify the morphology and composition of the glass alteration products. Prior to inspection the powders were mounted in resin and ground back before polishing. The mounted samples were carbon coated to prevent charging. The accelerating voltage was 15 kV and a working distance of 7-9 mm was used.

PHREEQC geochemical modelling [19] was used to calculate the saturation indices of potential leachate phases. The measured concentrations of the elements in the leachate were inputted into PHREEQC, which then calculated the saturation indices using the Lawrence Livermore National Laboratory (LLNL) thermodynamic database.

3. Results

3.1 MAS-NMR Spectroscopy

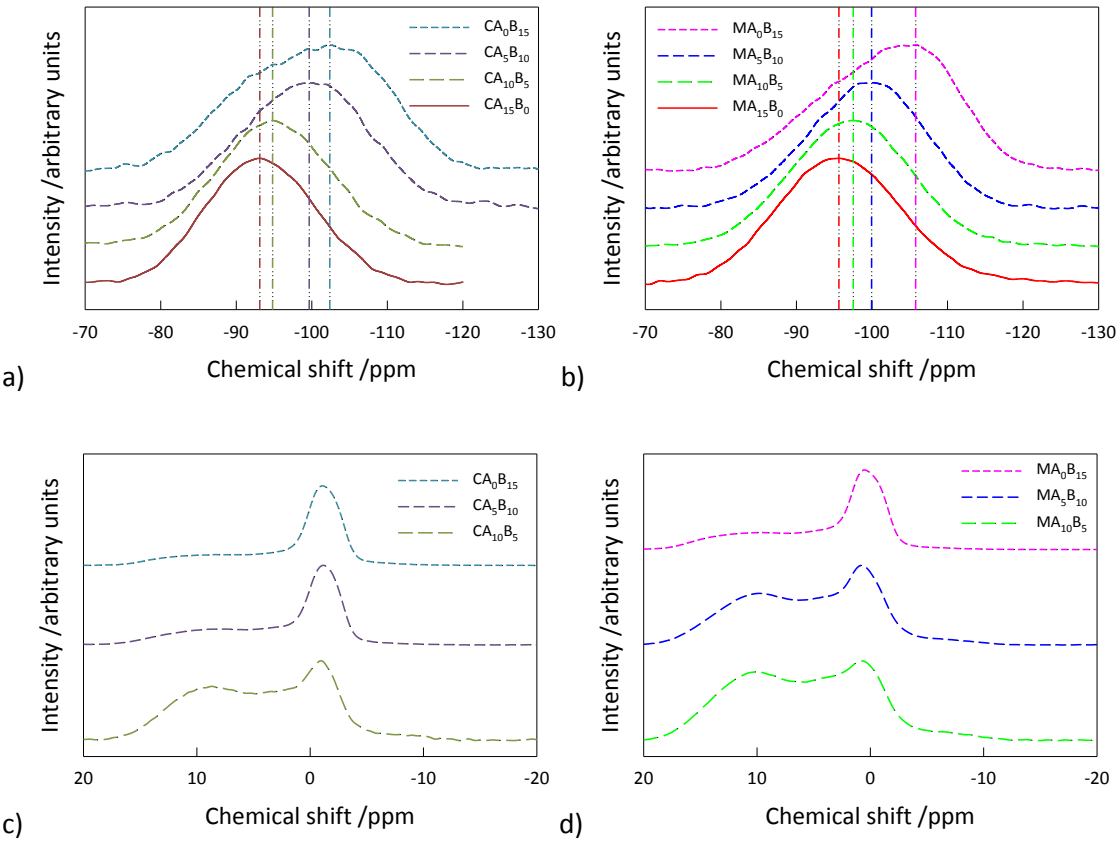

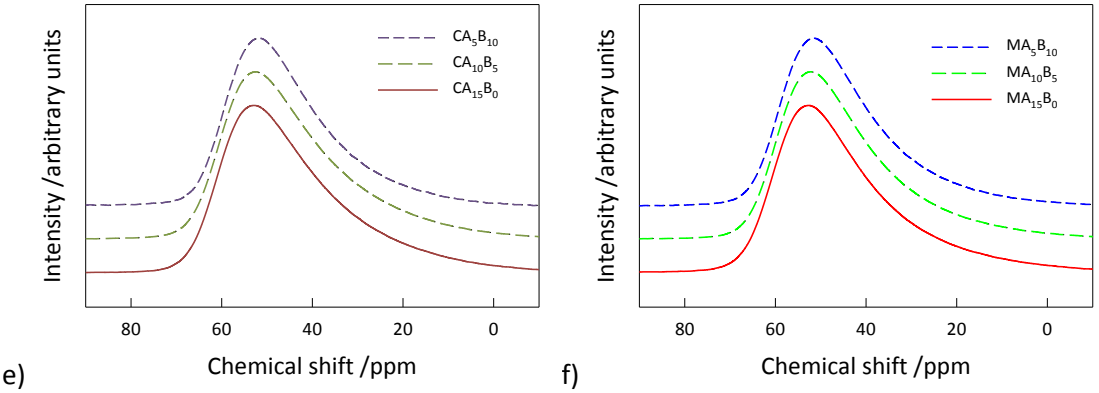

Figure 1. MAS-NMR: ^{29}Si spectra for (a) $CA_{15-x}B_x$ and (b) $MA_{15-x}B_x$ glasses; ^{11}B spectra for (c) $CA_{15-x}B_x$ and (c) $MA_{15-x}B_x$ glasses; ^{27}Al spectra for (e) $CA_{15-x}B_x$ and (f) $MA_{15-x}B_x$ glasses. All spectra are normalised to the maximum peak height

Table 2. Summary of results from ^{11}B, ^{27}Al and ^{29}Si MAS-NMR spectroscopy.

Glass	$B_2O_3/(Al_2O_3+B_2O_3)$	N_3	N_4	^{27}Al chemical shift /ppm	^{29}Si chemical shift /ppm
$CA_{15}B_0$	0.00	-	-	52.80	–93.13
$CA_{10}B_5$	0.32	0.875 ± 0.008	0.125 ± 0.008	52.56	–94.82
CA_5B_{10}	0.71	0.611 ± 0.002	0.389 ± 0.002	51.83	–99.68
CA_0B_{15}	1.00	0.542 ± 0.002	0.458 ± 0.002	-	–102.38
$MA_{15}B_0$	0.00	-	-	52.56	–95.65
$MA_{10}B_5$	0.33	0.912 ± 0.004	0.088 ± 0.004	52.07	–97.55
MA_5B_{10}	0.51	0.858 ± 0.007	0.142 ± 0.007	51.58	–99.97
MA_0B_{15}	1.00	0.622 ± 0.007	0.378 ± 0.024	-	–105.79

The ^{29}Si, ^{11}B and ^{27}Al MAS-NMR spectra for all the glasses investigated are shown in Figure 1. Both $CA_{15-x}B_x$ and $MA_{15-x}B_x$ glasses show an increasingly negative peak shift in the ^{29}Si MAS-NMR spectra with increasing $B_2O_3/(Al_2O_3+B_2O_3)$ ratio (Figures 1a, b and Table 2). This suggests that there is an increase in the proportion of symmetric Q_4(4Si) species present with increasing $B_2O_3/(Al_2O_3+B_2O_3)$ ratio. The calculated contributions of the different B environments in each glass, derived from the ^{11}B MAS-NMR spectra (Figures 1c and d), are given in Table 2. The values were corrected to account for loss of intensity from the ^{III}B contributions to the spinning sidebands, which does not occur for the ^{IV}B contributions [20]. The $CA_{10}B_5$ and $MA_{10}B_5$ spectra were fitted with one ^{IV}B peak, corresponding to ^{IV}B(1B, 3Si), as it was not possible to obtain a reasonable fit with two ^{IV}B peaks. In both Mg- and Ca-bearing glasses, the fraction of 4-coordinated B (N_4) was observed to increase with increasing $B_2O_3/(Al_2O_3+B_2O_3)$ ratio. In the Ca-containing glass compositions only, there was shift of

the ^{IV}B contribution of the ^{11}B spectra towards more negative relative frequencies with increasing $B_2O_3/(Al_2O_3+B_2O_3)$ ratio. This could be due to an increase in the amount of ^{IV}B(0B, 4Si) units in the glass.

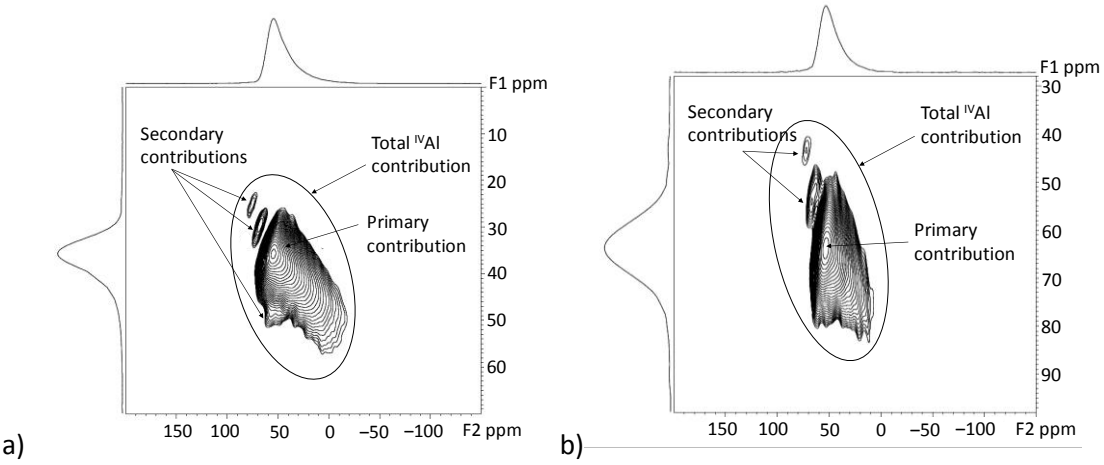

Figure 2. ^{27}Al 3QMAS-NMR spectra for: (a) $CA_{15}B_0$; and (b) CA_5B_{10} glasses.

The co-ordination environment of Al in compositions $CA_{15}B_0$ and CA_5B_{10} was investigated using ^{27}Al 3QMAS-NMR, as shown in Figure 2. The data indicate that Al was only present in tetrahedral coordination. In addition to the large primary ^{IV}Al contribution in the 3QMAS spectrum (at 58 to 27 ppm F1, 70 to –20 ppm F2, Fig. 2a), there appear to be three other features in the spectrum: a small peak at 29 – 23 ppm F1, 85 – 70 ppm F2; a slightly larger peak at 34 to 26 ppm F1, 80 to 60 ppm F2; and a shoulder in the primary contribution at 49 ppm F1, 55 ppm F2. This suggests that four different ^{IV}Al environments contribute to this spectrum. As the lineshapes for the $MA_{15-x}B_x$ ^{27}Al MAS-NMR spectra are very similar to those for the $CA_{15-x}B_x$ glasses, it is likely that Al in these glasses is also in predominantly tetrahedral coordination.

3.2 PCT-B Dissolution Experiments

The pH of the blank solutions ranged between pH 12.5 ± 0.1 and pH 13.7 ± 0.1. The pH(RT) values for solutions in contact with glass generally remained high throughout the experiments, with a starting value of pH 12.5 ± 0.1 and a value of pH 11.5-12.7 at the end of the experiment for the $CA_{15-x}B_x$ glasses and 11.2 for the $MA_{15-x}B_x$ glasses. However for $CA_{15}B_0$, $MA_{15}B_0$ and MA_0B_{15} lower values of ~8.5 were recorded. A pH value of ~8.5 was also obtained for a few time points in the middle of the experiment with some of the other glasses. It is therefore thought that these lower values were not present during the experiment, but rather arise from carbonation occurring once the solution had been removed from the glovebox, as some pH measurements were made outside the glovebox.

The normalised mass losses of B, Na, Al and Si as a function of glass composition and dissolution time are shown in Figures 3a to 3h for the 2 series of glasses.

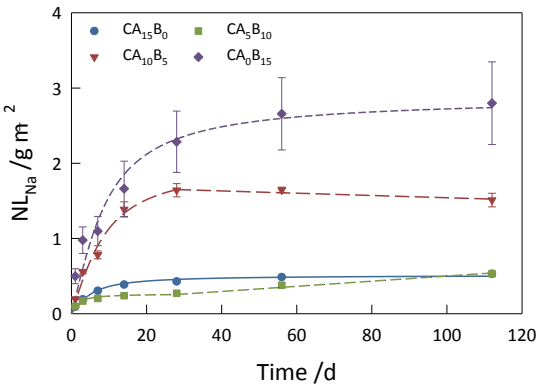

a)

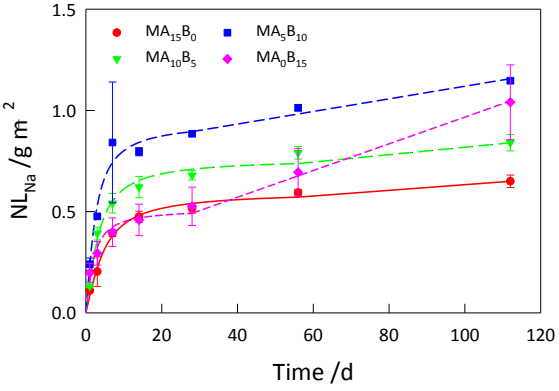

b)

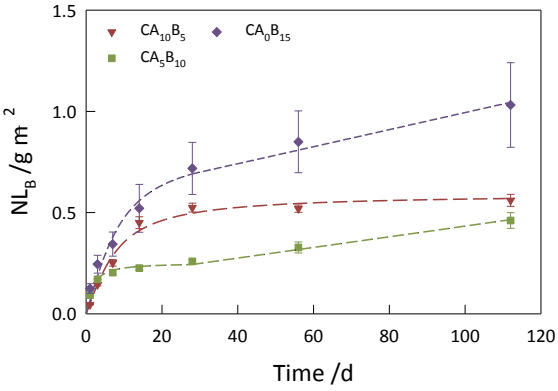

c)

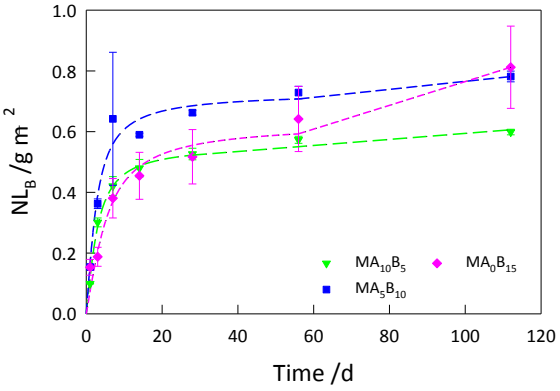

d)

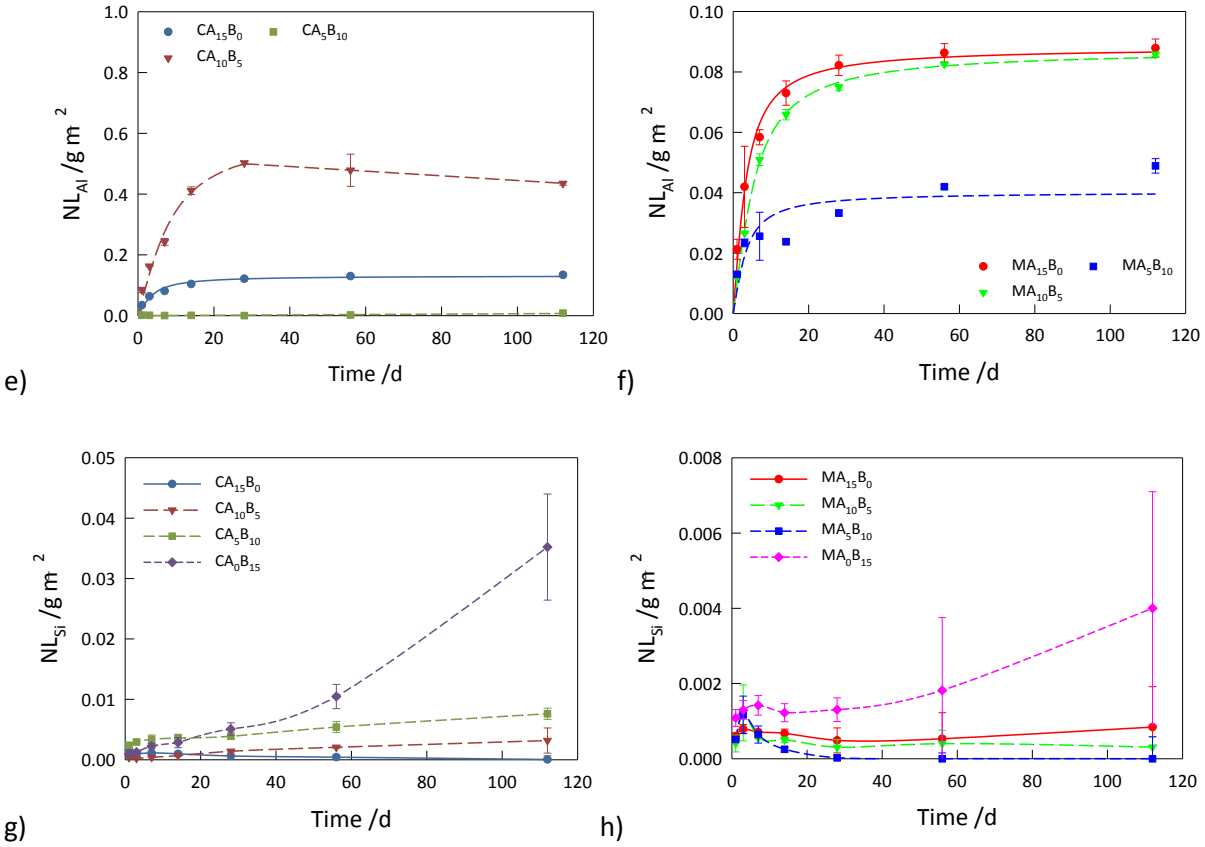

Figure 3. Leaching data for $CA_{15-x}B_x$ and $MA_{15-x}B_x$ glasses in saturated $Ca(OH)_2$ solutions at 50°C. Normalised mass losses of (a) & (b) Na, (c) & (d) B, (e) & (f) Al, (g) & (h) Si. Lines are fits to the data as detailed in the text.

For Na, B and Al the normalised loss data was empirically fitted with

$$NL_i = A\tan^{-1}\frac{t}{B} \qquad (2)$$

where *A* and *B* are fitting constants, which we have found provides a good empirical fit to the normalised loss data for a number of glasses, including the international simple glass (ISG)[21]. For this fit the normalised release rates are given by

$$NR_i = \frac{AB}{B^2 + t^2} \qquad (3)$$

For $CA_{10}B_5$ glass there is evidence of rate resumption in the Na and B data; the Al data actually starts to show a rate decrease. Similarly there is evidence of rate resumption in the B data for CA_5B_{10} glass and in the Na and B data for the $MA_{15-x}B_x$ glasses. In these cases equation (2) does not provide a good fit for longer times. In such cases the longer time data has been fitted using a straight line *i.e.*

$$NL_i = C + Dt \qquad (4)$$

where *C* and *D* are fitting constants. The fits made using equation (4) have been forced to be continuous in NL_i with the fits obtained using equation (2). In these cases the normalised release rate at long times is given by

$$NR_i = D. \quad (5)$$

It should be noted that where 2 fits are used although the NL_i fits are continuous (equations (2) and (4)) the resultant NR_i values (equations (3) and (4)) are not. The overall empirical fits made using equations (2) and (4) for Na and B were generally good (see figures 3a-d), whereas for Al the fits were poorer (figures 3e-f), particularly for the lowest normalised losses.

Figures 3g-h show that Si does not exhibit the conventional rate drop behaviour, there tends to be a small maximum in NL_{Si} at between 3 and 7 days after which NL_{Si} starts to decline. This decline continues for $CA_{15}B_0$, $MA_{10}B_5$ and MA_5B_{10}. For all the other glasses studied the NL_{Si} value then passes through a minimum before starting to increase again, with CA_0B_{15} exhibiting a particularly marked increase. As a results of this behaviour and the very low NL_{Si} values, due to the formation of Si containing alteration products, it was not possible to reliably fit this data using equation (2) and thus a spline fit has been used to guide the eye (figures 3g-h).

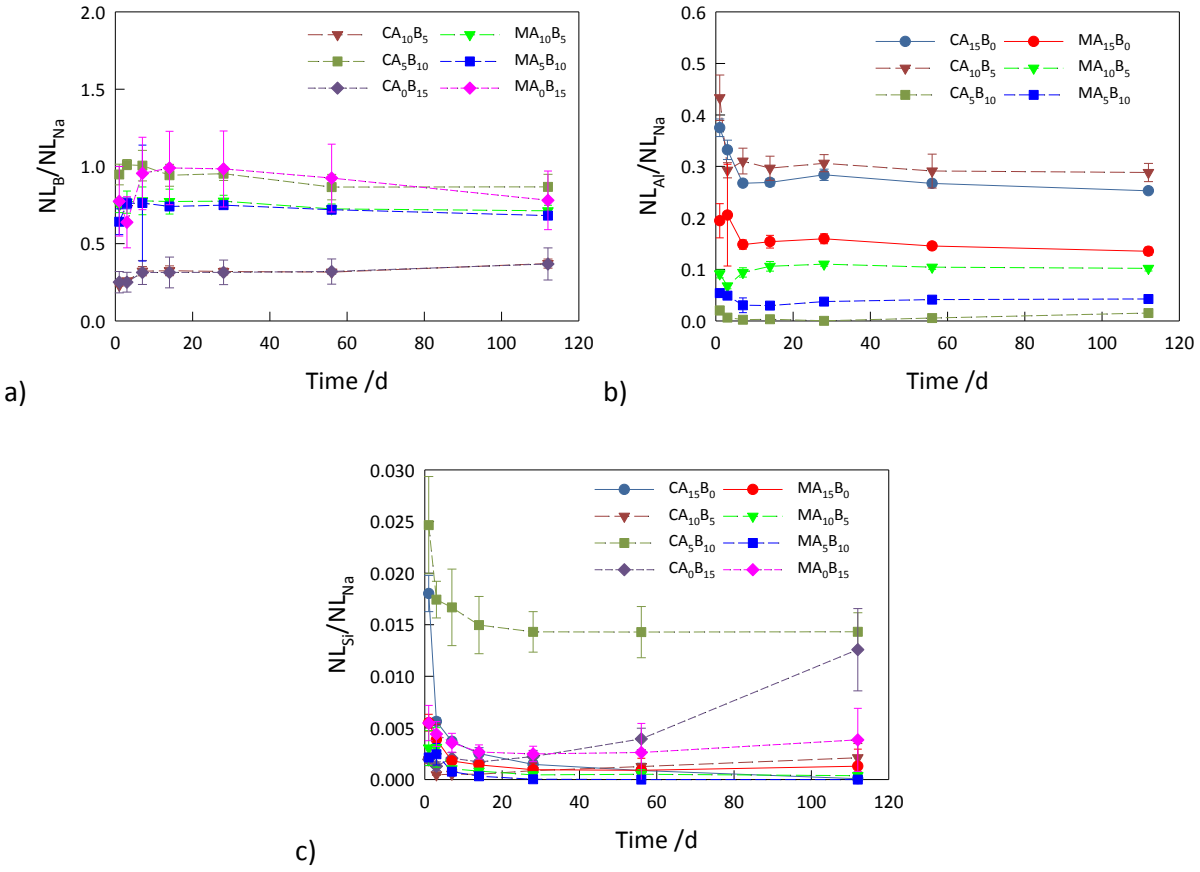

Figure 4: Normalised loss ratios as function of time for all the glasses studied a) NL_B/NL_{Na}, b) NL_{Al}/NL_{Na} and c) NL_{Si}/NL_{Na}; lines are drawn as a guide to the eye and are not fits

Figures 4 shows that leaching was apparently incongruent for Na, B, Al and Si; the NL_{Si}/NL_{Na} (Figure 4c) are particularly low reflecting the fact that silica was involved in the formation of alteration phases in the system. Leaching rates for Na calculated using equations (3) and (5) as appropriate are shown in figure 5 and the NL_i values for both Na and B at 0 d and 112 d are given in Table 3. The discontinuity in the calculated NL_i values indicates resumption of alteration can be clearly seen for all of the $MA_{15-x}B_x$ glasses. The situation is more complicated for the $CA_{15-x}B_x$ glasses where only CA_5B_{10} clearly shows evidence of resumption; for $CA_{10}B_5$ the fitted line has a negative slope and thus cannot be shown on the log linear plot used in figure 5.

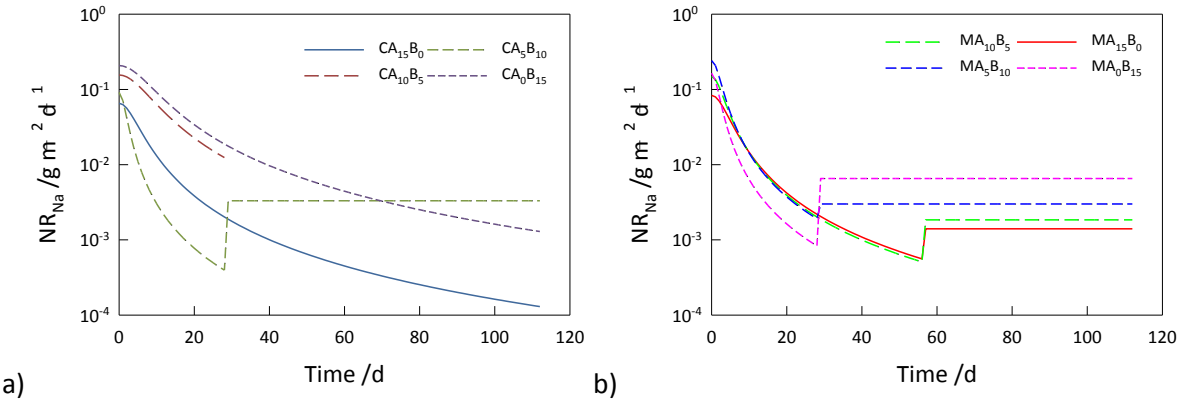

Figure 5. Calculated sodium leaching rates for (a) $CA_{15-x}B_x$ and (b) $MA_{15-x}B_x$ glasses. The step to a constant rate indicates a resumption of alteration. The $CA_{10}B_5$ data exhibits a negative rate at longer times and thus cannot be plotted on a logarithmic axis.

Table 3. Normalised mass loss rates at 0 d and 112 d for Na and B in saturated $Ca(OH)_2$ solutions for for all of the glasses.

	Rate /g m^{-2} d^{-1}							
Glass	**$CA_{15}B_0$**	**$CA_{10}B_5$**	**CA_5B_{10}**	**CA_0B_{15}**	**$MA_{15}B_0$**	**$MA_{10}B_5$**	**MA_5B_{10}**	**MA_0B_{15}**
$NR_{Na}(0)$	(6.6 ± 0.8) × 10^{-2}	(1.6 ± 0.3) × 10^{-1}	(9.2 ± 1.7) × 10^{-2}	(2.1 ± 0.5) × 10^{-1}	(8.3 ± 0.9) × 10^{-2}	(1.5 ± 0.2) × 10^{-1}	(2.4 ± 0.5) × 10^{-1}	(1.6 ± 0.4) × 10^{-1}
$NR_{Na}(112)$	(1.3 ± 0.2) × 10^{-4}	(−1.5 ± 0.3) × 10^{-3}	(3.4 ± 0.3) × 10^{-3}	(1.3 ± 0.2) × 10^{-3}	(1.4 ± 0.4) × 10^{-3}	(1.8 ± 1.0) × 10^{-3}	(3.1 ± 0.3) × 10^{-3}	(6.6 ± 0.3) × 10^{-3}
$NR_B(0)$	-	(5.1 ± 0.7) × 10^{-2}	(9.5 ± 1.4) × 10^{-2}	(6.5 ± 1.8) × 10^{-2}	-	(1.2 ± 0.1) × 10^{-1}	(1.7 ± 0.3) × 10^{-1}	(7.5 ± 1.8) × 10^{-2}
$NR_B(112)$	-	(2.6 ± 0.2) × 10^{-3}	(4.2 ± 0.4) × 10^{-3}	(3.4 ± 0.2) × 10^{-3}	-	(1.0 ± 0.2) × 10^{-3}	(1.3 ± 0.4) × 10^{-3}	(3.9 ± 0.9) × 10^{-3}

3.3 Alteration layer analysis

SEM micrographs, including elemental maps, and EDS analyses of alteration layers formed on the surface of particles of the calcium bearing $CA_{15-x}B_x$ glasses reacted for 112 days in $Ca(OH)_2$ are shown in Figure 6. For the composition $CA_{15}B_0$ (Fig. 6a), thin (~1-2 µm) alteration layers, primarily containing Ca and Si, with a minor amount of Al were observed to form on the surface of particles. Additionally, a phase containing Ca, Si, and Al was observed. As these layers are thin and the EDS trace includes a strong C signal, indicating a significant contribution from the surrounding resin, the presence of Na from the glass cannot be definitely be ruled out, although the relative Ca content has clearly increased. The presence of glass-forming elements indicates that this may have been detached from the sample surface. The alteration layers observed on the surface of the $CA_{10}B_5$ and CA_5B_{10} (Figs. 6b-c, respectively) glass compositions were similar to $CA_{15}B_0$, containing Ca, Si, Al, and O. The thickness of the alteration layer for these 2 glasses was a bit larger, ranging from 5-10 µm. The alteration layer on the surface of the CA_0B_{15} particles (Figure 6d) was again similar being ~5 µm thick but in this case the layer did not contain Al.

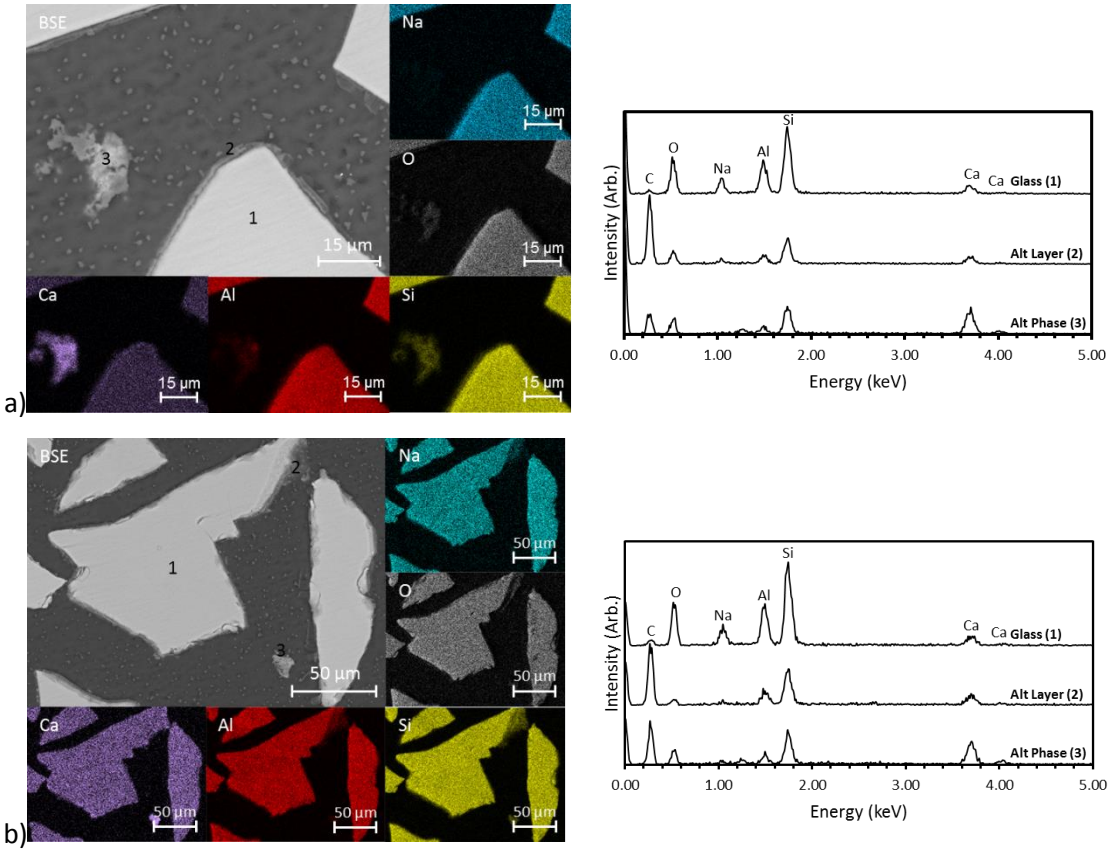

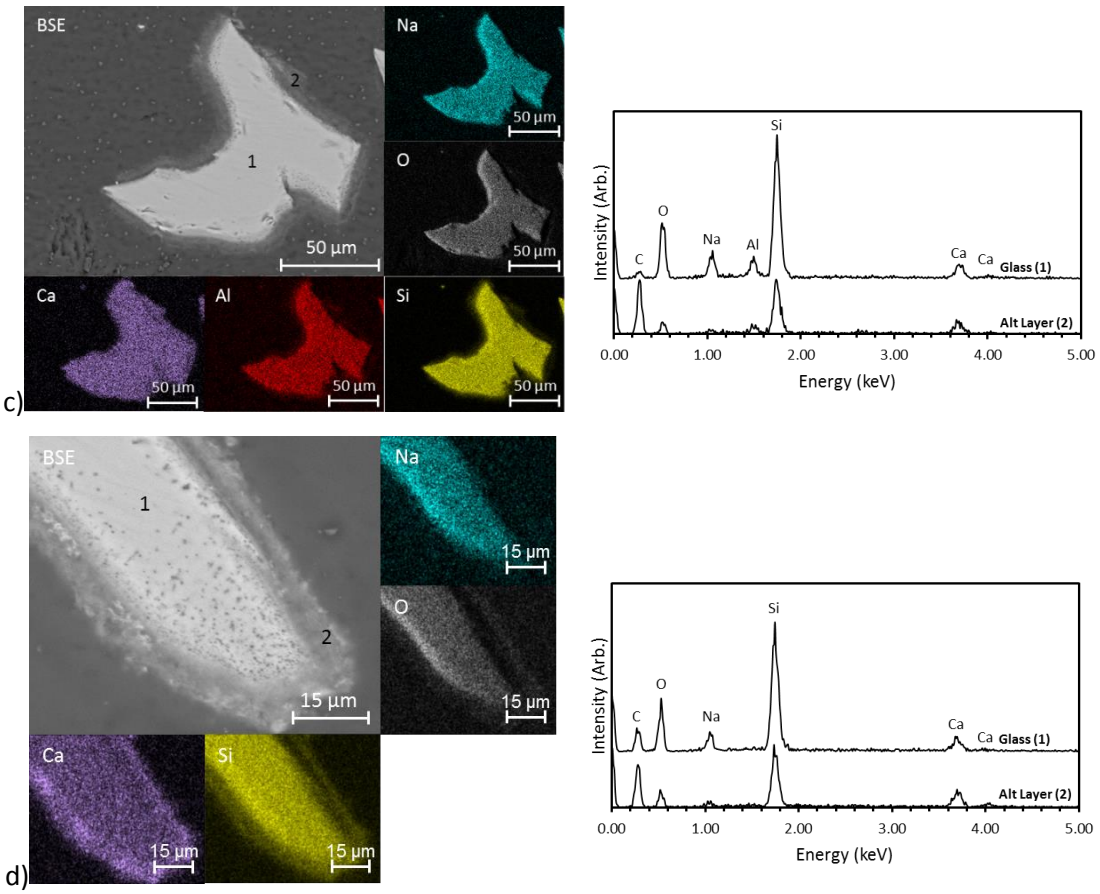

Figure 6. BSE micrographs, elemental maps and EDS spectra of: (a) $CA_{15}B_0$; (b) $CA_{10}B_5$; (c) CA_5B_{10} and (d) CA_0B_{15} particles after 112 days leaching in saturated $Ca(OH)_2$ solution.

SEM/EDS mapping of particles from the Mg-bearing $MA_{15-x}B_x$ glasses are shown in Figure 7. The morphology and composition of the layers were similar to those observed for the $CA_{15-x}B_x$ glasses, ranging in the thickness from 1 to 10 µm, and composed of Ca, Si, and Al (except for MA_0B_{15}), however they were also observed to contain Mg. Furthermore, several additional, and compositionally distinct, phases were observed for the Mg-bearing glasses, that were not observed for the Ca-bearing glass compositions. For example, analysis of $MA_{10}B_5$ (Fig. 7b) demonstrated the presence of a Ca-Al phase (labelled 3, Fig. 7b) and a Ca-Si phase containing Mg and Al (labelled 4, Fig. 7b). The Ca-Al phase appeared to be similar in morphology and composition to the Ca- and Al-rich phase observed on the $MA_{15}B_0$ sample. Three different alteration phases were observed on the MA_5B_{10} particles, characterised by their Mg content: a Ca-Si phase containing virtually no Mg (< 0.1 at.%) (labelled 2, Fig. 6c); a phase containing an intermediate quantity of Mg (2.0 – 2.5 at.%) (labelled 3, Fig. 6c); and a phase containing an elevated quantity of Mg (> 4.5 at.%) (labelled 4, Fig. 6c). Again the strength of the C signal, indicating a significant contribution from the surrounding resin, means that the presence of Na in these layers cannot be definitely be ruled out.

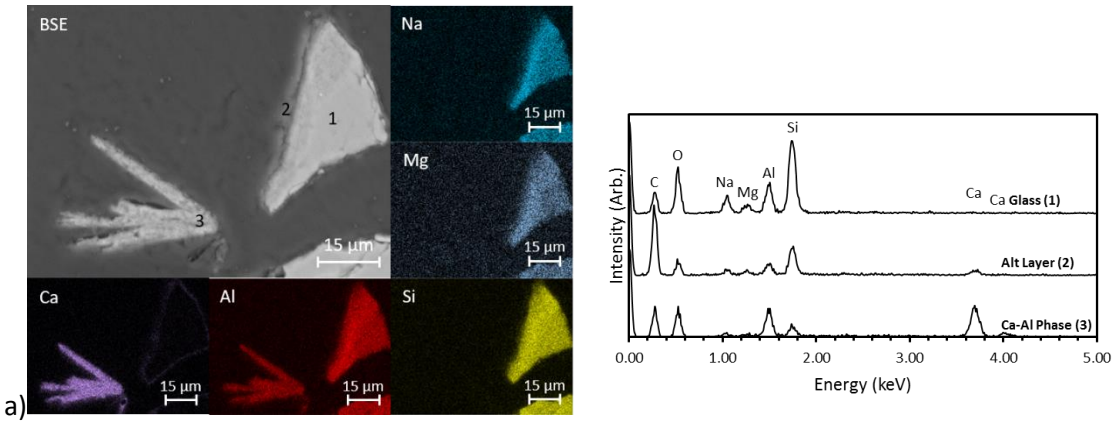
a)
BSE
Na
Mg
Ca
Al
Si
15 µm
1
2
3
Intensity (Arb.)
Energy (keV)
C
O
Na
Mg
Al
Si
Ca
Ca Glass (1)
Alt Layer (2)
Ca-Al Phase (3)
0.00
1.00
2.00
3.00
4.00
5.00

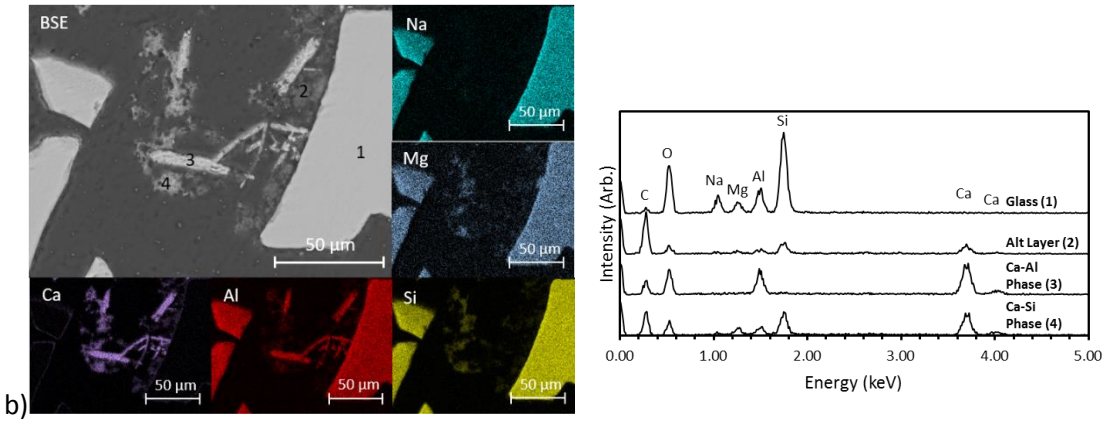
b)
BSE
Na
Mg
Ca
Al
Si
50 µm
1
2
3
4
Intensity (Arb.)
Energy (keV)
C
O
Na
Mg
Al
Si
Ca
Ca Glass (1)
Alt Layer (2)
Ca-Al Phase (3)
Ca-Si Phase (4)
0.00
1.00
2.00
3.00
4.00
5.00

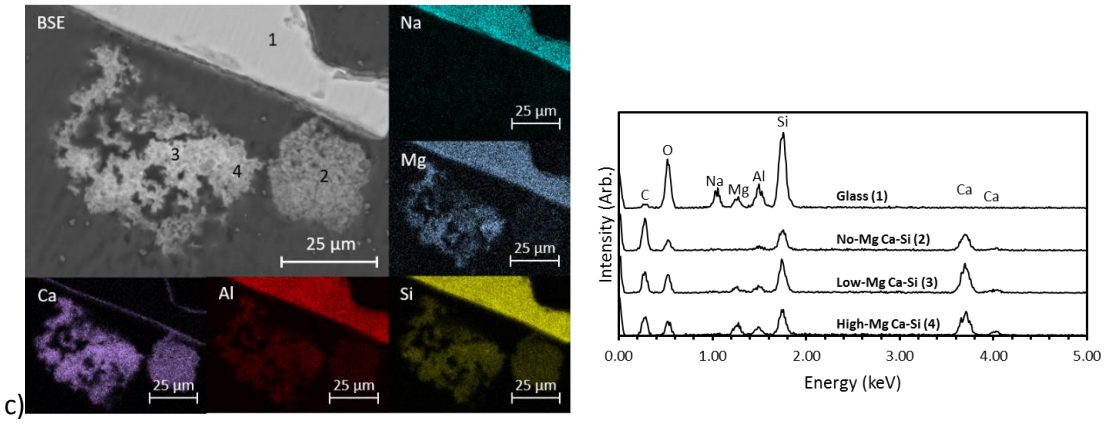
c)
BSE
Na
Mg
Ca
Al
Si
25 µm
1
2
3
4
Intensity (Arb.)
Energy (keV)
C
O
Na
Mg
Al
Si
Ca
Glass (1)
No-Mg Ca-Si (2)
Low-Mg Ca-Si (3)
High-Mg Ca-Si (4)
0.00
1.00
2.00
3.00
4.00
5.00

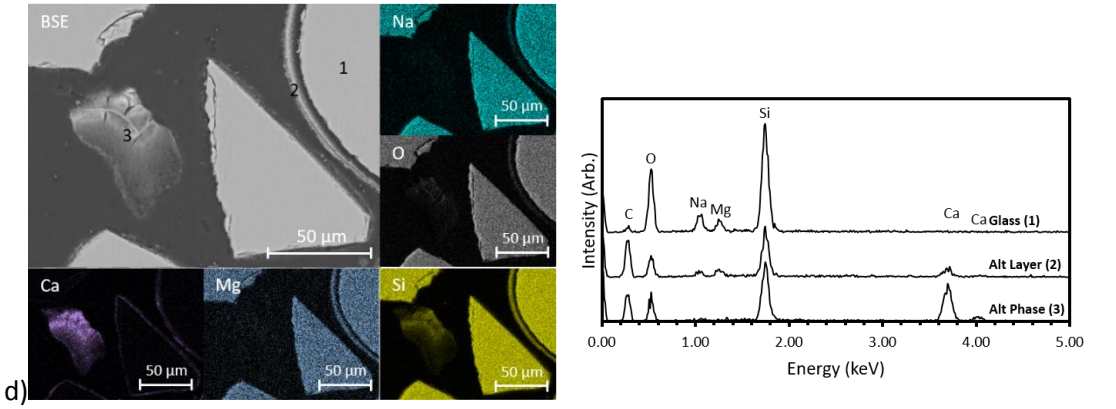
d)
BSE
Na
O
Ca
Mg
Si
50 µm
1
2
3
Intensity (Arb.)
Energy (keV)
C
O
Na
Mg
Si
Ca
Ca Glass (1)
Alt Layer (2)
Alt Phase (3)
0.00
1.00
2.00
3.00
4.00
5.00

Figure 7. BSE micrographs, elemental maps and EDS spectra of: (a) $MA_{15}B_0$; (b) $MA_{10}B_5$; (c) MA_5B_{10} and (d) MA_0B_{15} particles after 112 days leaching in saturated $Ca(OH)_2$ solution.

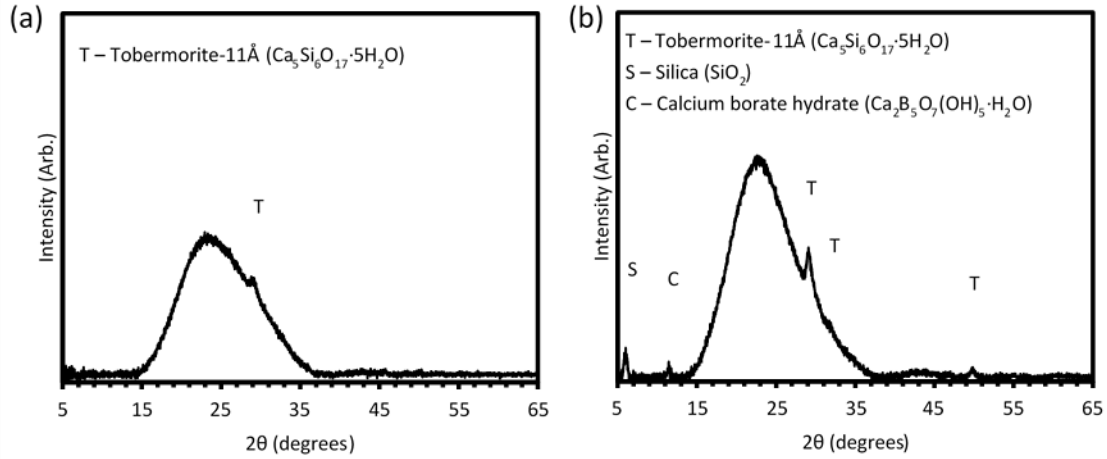

Figure 8. X-ray Diffraction patterns for: (a) CA_5B_{10}; and (b) MA_5B_{10} samples after 112 days leaching in saturated $Ca(OH)_2$ solution.

X-ray diffraction analysis of CA_5B_{10} identified the presence of tobermorite-11Å (PDF [00-019-1364], $Ca_5Si_6O_{17}·5H_2O$) (Figure 8a). Tobermorites are classified based on the basal plane spacing which depends on the total water content [22]. The peak at approximately 29.2° 2θ corresponds to the major reflection of the tobermorite-11Å phase. No other crystalline phases were present in sufficient quantity on the CA_5B_{10} sample to be detected by this method. The diffraction pattern for MA_5B_{10} (Fig. 8b) shows that in addition to tobermorite-11Å, a calcium borate hydrate phase (PDF [00-052-1654], $Ca_2B_5O_7(OH)_5·H_2O$) may also be present.

4. Discussion

4.1 Effect of Glass Composition on Structure

4.1.1 Effect of Varying B/Al ratio

The ^{29}Si NMR peaks moved to more negative chemical shift values with increasing B/Al ratio for both the $CA_{15-x}B_x$ and $MA_{15-x}B_x$ glasses (Table 2). This may be due to either: (i) the formation of fewer Si-O-Al bonds because of the decrease in Al_2O_3 content; or (ii) an increase in the proportion of symmetric Q_4 species over Q_3 and asymmetric $Q_4(X)$ species. Fewer Si-O-Al bonds would be expected to result in a decrease in chemical shift, as the Si nuclei in silicate tetrahedra are less shielded when they involve Si-O-Al bonds instead of Si-O-Si or Si-O-B bonds [20]. An increase in the proportion of symmetric Q_4 species probably arises because in three of the four B containing glasses ~85-90% of the B is present in trigonal rather than tetragonal coordination and in the remaining case ~60% of the B is present in

trigonal coordination (see table 2). Meanwhile the 3QMAS-NMR spectra indicate that the Al is mostly present in tetrahedral coordination, because Al is more readily charge compensated than B [23,24,25]. From the measured compositions (Table 1) and the measured N_4 values (Table 2) it is calculated that the overall tetrahedral unit content of the glasses decreases with increasing B (decreasing Al) content. In addition the fraction of tetrahedral units that are silicate units increases. These changes will result in a decrease in the number of potential Si – O – X bonds (X = B, Al), as trigonal ^{III}B units can only bond to three other units, whereas ^{IV}B and ^{IV}Al can bond to four. Thus, the replacement of Al_2O_3 by B_2O_3 leads to a decrease in the total number of Q_4(X) units and an increase in symmetric Q_4 units.

The fraction of ^{IV}B units in the $CA_{15-x}B_x$ and $MA_{15-x}B_x$ glasses increased as a function of the B/Al ratio (Table 2). This effect has been previously observed by Geisinger *et al.* in glasses along the $NaAlSi_3O_8$-$NaBSi_3O_8$ join [26]. Based on the measured compositions (Table 1) and N_4 values (Table 2) it is calculated that some of the charge compensation for Al and B must be provided by the alkaline earth cations for 5 out of the 8 glasses (CA_5B_{10}, CA_0B_{15} and MA_0B_{15} are the exceptions). The 3QMAS-NMR spectra for $CA_{15}B_0$ and CA_5B_{10} suggest the presence of 3-4 different ^{IV}Al environments. These are likely to arise from other SiO_4 and AlO_4 units to which the ^{IV}Al tetrahedron is bonded [27]. The largest contribution (Fig. 2) is probably due to ^{IV}Al units bonded to four SiO_4 tetrahedra, denoted ^{IV}Al(4Si), due to the avoidance of ^{IV}Al – O – ^{IV}Al bonds (the Loewenstein Avoidance Principle [28]). The two smaller peaks probably correspond to: ^{IV}Al(3Si) and ^{IV}Al(2Si) (at 34 – 26 ppm F1, 80 – 60 ppm F2 and 29 – 23 ppm F1, 85 – 70 ppm F2, respectively). The former consists of an AlO_4 tetrahedron connected to three SiO_4 units and one AlO_4 while the latter consists of an AlO_4 tetrahedron linked to two SiO_4 and two AlO_4 units. The cause of the shoulder in the primary ^{IV}Al(4Si) contribution at around 49 ppm F1, 55 ppm F2 is not known.

4.1.2 Effect of Alkaline-Earth Ions

Systematic differences are observable between the ^{29}Si and ^{11}B spectra of the $CA_{15-x}B_x$ and $MA_{15-x}B_x$ series. The ^{29}Si chemical shift is more negative for each of the $MA_{15-x}B_x$ glasses compared to their $CA_{15-x}B_x$ counterparts. The fraction of ^{IV}B units tends to be higher for the $CA_{15-x}B_x$ glasses than for the $MA_{15-x}B_x$ glasses (Table 2). However the biggest difference in ^{IV}B fraction seen between equivalent glasses (CA_5B_{10} and MA_5B_{10}) is probably also affected by the much lower Al content in the CA_5B_{10} glass (see Table 1). This means that all of the charge compensation (for both Al and the measured N_4) in the CA_5B_{10} glass can be supplied by Na^+ ions rather than some of it being provided by alkaline earth ions. Lower ^{IV}B would lead to lower numbers of Si – O – B bonds and hence fewer asymmetric Q_4 silicate tetrahedra, resulting in more negative ^{29}Si spectral shifts.

Some recent work by Guo *et al.* [29] has suggested that ^{VI}Al units can be found in 5-6 component aluminoborosilicate glasses, with the content varying with the identity of the alkaline earth cation. However only minor differences between the ^{27}Al spectra for the Ca-containing and Mg-containing glasses were identified in the current work, suggesting that the Al is fully charge-compensated in all the glasses studied. This discrepancy is probably due to the significant differences in overall chemical composition of the glasses studied.

4.2 Effect of Glass Composition on Dissolution in $Ca(OH)_2$

Na was used as a tracer for overall glass dissolution as it was present in all glasses (unlike B), and was not observed to be significantly retained in secondary phases. The potential detection of a calcium borate hydrate phase (PDF [00-052-1654], $Ca_2B_5O_7(OH)_5{\cdot}H_2O$) in the MA_5B_{10} sample (a possibility previously suggested by Utton *et al.* [9]) also calls into question the efficacy of using boron as a "tracer" element for glass dissolution under high-pH, Ca-rich conditions. There is some indication that the dissolution losses, as assessed by Na, tended to increase with $[B_2O_3]/([Al_2O_3]+[B_2O_3])$ for both the Mg-and Ca-bearing glasses as shown in Figure 9, although this dependence is not completely clear cut. Enhanced rates of dissolution with increasing $[B_2O_3]/([Al_2O_3]+[B_2O_3])$ may be attributed to the lower resistance of Si – O – B bonds to hydrolysis compared to Si – O – Al bonds [2]. The decrease in non-silicate tetrahedral units (^{IV}B + ^{IV}Al), due to the replacement of tetrahedral Al on a molar basis by B, of which <50% is in tetrahedral coordination, may also enhance dissolution rates. Previous work by Pierce *et al.* [30] suggested that the initial rate of dissolution of sodium aluminoborosilicate glasses, as calculated from dynamic, Single-Pass Flow-Through (SPFT) dissolution experiments, should remain approximately constant with varying B/Al ratio, even at pH values of around 12. This behaviour is not obviously seen with either of the two sets of glasses studied. This could indicate that the conditions in the PCT-B experiments, even at the earliest sampling points, are not far enough from equilibrium to negate solution saturation effects on the dissolution rate.

The dependence of the dissolution results on the B/Al ratio potentially has implications for the use of natural and synthetic basalts as analogues of nuclear waste glasses [31]. Basaltic compositions do not contain B_2O_3 whereas many nuclear waste glasses do (see, for example, [32]). Thus mechanistic differences arising from the presence of B_2O_3 cannot be ignored in evaluating the long term durability performance of such glasses.

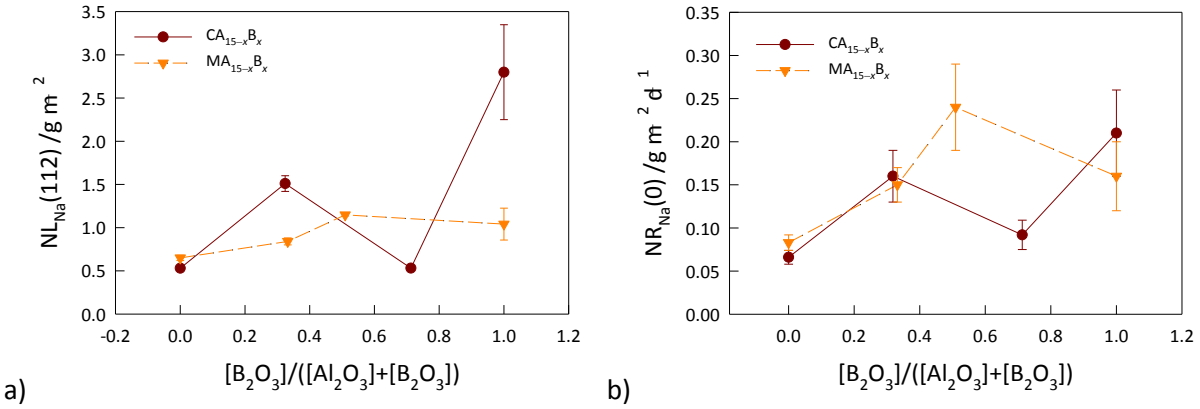

Figure 9. Variation of a) the normalised mass loss of sodium at 112 days and b) the initial normalised loss of Na rate versus the $[B_2O_3]/([Al_2O_3]+[B_2O_3])$ content. Lines drawn as a guide to the eye.

Table 4. Ca/Al ratios for the calcium aluminate phases observed in the $MA_{1-x}B_x$ samples, per triplicate EDS spot analysis.

Sample	Ca/Al (At. %)	Equivalent CaO/Al_2O_3
$MA_{15}B_0$	1.74 ± 0.05	3.47 ± 0.11
$MA_{10}B_5$	2.42 ± 0.25	4.83 ± 0.51
MA_5B_{10}	2.69 ± 0.01	5.37 ± 0.03

The measured normalised losses were similar for both Ca and Mg-containing glasses although some Ca-containing glasses exhibited higher corrosion rates than the Mg-containing ones (Figures 3-b). This result is unexpected based on broadly similar comparisons of Ca- and Mg-containing glasses in the literature [33,34]. It indicates that, at least with these glasses, the precipitation of Mg-containing secondary phases does not result in a significant difference in alteration rate at the early stages. There is evidence however of a greater tendency to rate resumption in the Mg containing glasses which may suggest that different ranking would be found at longer times. Hence further investigation is required before firm conclusions can be drawn. Precipitation of Mg-containing secondary phases during glass dissolution has been well documented [33,35,36,37] although the precipitation of secondary phases in a mixed Ca and Mg system has not been thoroughly investigated. The Ca- and Al-rich phase observed in the SEM / EDS analysis of the $MA_{15-x}B_x$ glasses is likely to be a calcium aluminate hydrate phase. However, if crystalline, this phase was not present in high enough concentration to be detected by X-ray diffraction (Fig. 8b). The Ca/Al ratios for this phase (Table 4) suggest that it could be C_4AH_{13} ($Ca_4Al_2O_7{\cdot}13H_2O$) or C_4AH_{19} ($Ca_4Al_2O_7{\cdot}19H_2O$). The PHREEQC calculations, utilising solution data from the dissolution of MA_5B_{10} in $Ca(OH)_2$, however suggest that C_4AH_{13} and C_4AH_{19} are unlikely to form in the presence of significant concentrations (>

10 ppm) of Mg and Si. Instead the calculations suggest that Mg-containing phases, such as saponite and sepiolite, which are aluminosilicate and silicate clay minerals, respectively, have higher saturation indices in solution and are therefore more likely to form than Ca-containing phases such as tobermorite. This is despite the calculations using Ca concentrations of 400 – 700 ppm, compared to Mg concentrations of 5 – 40 ppm. It should also be noted that the validity of PHREEQC is limited by the quality of thermodynamic data available on these phases. We therefore hypothesise that Mg-Si phases, such as those observed in Figure 7, precipitate first, followed by the precipitation of calcium aluminate hydrate phases. The precipitation of magnesium silicates has been previously observed by Corkhill *et al.* [17] who noted the formation of sepiolite ($Mg_4Si_6O_{15}(OH)_2{\cdot}6H_2O$) following alteration of the Mg-rich MW-25% glass in $Ca(OH)_2$. Sequential phase formation could explain why Ca-Al phases were present in the $MA_{15-x}B_x$ samples, but not in the $CA_{15-x}B_x$ samples. While it is thought that Ca-Si phases are formed preferentially to Ca-Al phases, the formation of Mg-Si phases in the $MA_{15-x}B_x$ samples will remove Si from solution suppressing Ca-Si phase formation resulting in the formation of Ca-Al phases instead. Different phase evolutions might also explain why the solution pH became slightly lower with the Mg containing glasses compared to the Ca containing glasses.

It should also be noted that the glasses considered here have relatively simple compositions compared to real nuclear waste glasses and there is increasing evidence that small changes in composition can lead to considerable differences in leaching behaviour [21,34].

5. Conclusions

Eight glasses with varying B_2O_3 and Al_2O_3 contents in the $Na_2O{\cdot}CaO{\cdot}(15–x)Al_2O_3{\cdot}xB_2O_3{\cdot}SiO_2$ ($CA_{15-x}B_x$) and $Na_2O{\cdot}MgO{\cdot}(15–x)Al_2O_3{\cdot}xB_2O_3{\cdot}SiO_2$ ($MA_{15-x}B_x$) systems were fabricated, and their structure and dissolution behaviour in high-pH, Ca-rich conditions were investigated. Increasing the $[B_2O_3]/([Al_2O_3]+[B_2O_3])$ ratio of the alkali-alkaline-earth aluminoborosilicate glasses led to an overall decrease in the proportion of non-silicate tetrahedral species ($^{IV}Al + {}^{IV}B$) and a decrease in Si – O – X bonds (X = B, Al). In addition, the Mg-containing glasses exhibited lower ^{IV}B fractions than their Ca-containing counterparts, which is thought to be due to the presence of ^{IV}Mg tetrahedra in the network, although this requires confirmation through ^{25}Mg MAS-NMR or Extended X-Ray Absorption Fine Structure (EXAFS) spectroscopy. That the Ca- and Mg-containing glasses were structurally different and behaved dissimilarly during dissolution in high-pH, Ca-rich conditions is important due to the existence of UK HLW vitrified product with significant quantities of Mg arising from Magnox waste. In addition, as the effect of B_2O_3 and Al_2O_3 contents on the structure and dissolution of

glasses is important this suggests that natural glasses, which contain no boron, may not be suitable natural analogues for nuclear waste glasses.

6. Acknowledgements

DJB acknowledges financial support from the EPSRC Nuclear FiRST CDT (EP/G037140/1) and CLC acknowledges EPSRC for the award of an ECR Fellowship (EP/N017374/1). NCH acknowledges support from the RAEng and the Nuclear Decommissioning Authority. We acknowledge support from the UK Government Department of Energy and Climate Change, through the award of the MIDAS Collaboratory, for analytical equipment. We thank Neil Bramall of the Department of Chemistry, University of Sheffield for ICP-AES compositional analysis of the glass samples and David Apperley and the EPSRC MAS-NMR service at the University of Durham for the NMR data.

References

[1] M. Harrison, B. Dunnett, S. Morgan, C. Scales, and J. Small, "International research on vitrified HLW long-term behaviour:state of the art," *NNL (09)8864*, no. 4, 2009.

[2] P. A. Bingham, N. C. Hyatt, and R. J. Hand, "Vitrification of UK intermediate level radioactive wastes arising from site decommissioning: Property modelling and selection of candidate host glass compositions," *Glass Technol. Eur. J. Glass Sci. Technol. Part A*, vol. 53, no. 3, pp. 83–100, 2012.

[3] N.J. Cassingham, C.L. Corkhill, M.C. Stennett, R.J. Hand, and N.C. Hyatt, Alteration layer formation of Ca- and Zn-oxide bearing alkali borosilicate glasses for immobilisation of UK high level waste: A vapour hydration study J. Nucl. Mater. 479 639-646 (2016) DOI: 10.1016/j.jnucmat.2016.06.009

[4] B. Thien, N. Godon, F. Hubert, F. Angéli, S. Gin, and A. Ayral, "Structural identification of a trioctahedral smectite formed by the aqueous alteration of a nuclear glass," *Appl. Clay Sci.*, vol. 49, no. 3, pp. 135–141, 2010.

[5] B. Thien, N. Godon, A. Ballestero, S. Gin, and A. Ayral, "The dual effect of Mg on the long-term alteration rate of AVM nuclear waste glasses," *J. Nucl. Mater.*, vol. 427, no. 1–3, pp. 297–310, 2012.

[6] E. Curti, R. Dähn, F. Farges, and M. Vespa, "Na, Mg, Ni and Cs distribution and speciation after long-term alteration of a simulated nuclear waste glass: A micro-XAS/XRF/XRD and wet chemical study," *Geochim. Cosmochim. Acta*, vol. 73, no. 8, pp. 2283–2298, 2009.

[7] P. Frugier, C. Martin, I. Ribet, T. Advocat, and S. Gin, "The effect of composition on the leaching of three nuclear waste glasses: R7T7, AVM and VRZ," *J. Nucl. Mater.*, vol. 346, no. 2–3, pp. 194–207, 2005.

[8] T. Chave, P. Frugier, S. Gin, and A. Ayral, "Glass-water interphase reactivity with calcium rich solutions," *Geochim. Cosmochim. Acta*, vol. 75, no. 15, pp. 4125–4139, 2011.

[9] C. A. Utton, R. J. Hand, P. A. Bingham, N. C. Hyatt, S. W. Swanton, and S. J. Williams, "Dissolution of vitrified wastes in a high-pH calcium-rich solution," *J. Nucl. Mater.*, vol. 435, no. 1–3, pp. 112–122, 2013.

[10] Department of Energy & Climate Change. *2014 White Paper: Implementing Geological Disposal*. (2014).

[11] ONDRAF/NIRAS. Research, Development and Demonstration (RD&D) "Plan for the geological disposal of high-level and/or long-lived radioactive waste including irradiated fuel of considered as waste, State-of-the-art report as of December 2012." *ONDRAF/NIRAS, Rep. NIROND-TR 2013-12 E* 413, 2013.

[12] S. Gin and J. P. Mestre, "SON 68 nuclear glass alteration kinetics between pH 7 and pH 11.5," *J. Nucl. Mater.*, vol. 295, no. 1, pp. 83–96, 2001.

[13] P. K. Abraitis, F. R. Livens, J. E. Monteith, J. S. Small, D. P. Trivedi, D. J. Vaughan and R. A. Wogelius, "The kinetics and mechanisms of simulated British Magnox waste glass dissolution as a function of pH, silicic acid activity and time in low temperature aqueous systems," *Appl. Geochemistry*, vol. 15, no. 9, pp. 1399–1416, 2000.

[14] J. P. Hamilton, S. L. Brantley, C. G. Pantano, L. J. Criscenti, and J. D. Kubicki, "Dissolution of nepheline, jadeite and albite glasses: Toward better models for aluminosilicate dissolution," *Geochim. Cosmochim. Acta*, vol. 65, no. 21, pp. 3683–3702, 2001.

[15] E. M. Pierce, E. A. Rodriguez, L. J. Calligan, W. J. Shaw, and B. Pete McGrail, "An experimental study of the dissolution rates of simulated aluminoborosilicate waste glasses as a function of pH and temperature under dilute conditions," *Appl. Geochemistry*, vol. 23, no. 9, pp. 2559–2573, 2008.

[16] C. A. Utton, R. J. Hand, N. C. Hyatt, S. W. Swanton and S. J. Williams, "Formation of alteration products during dissolution of vitrified ILW in a high-pH calcium-rich solution" *J. Nucl. Mater.* **442** (2013) 33-45 DOI: 10.1016/j.jnucmat.2013.08.026

[17] C. L. Corkhill, N. J. Cassingham, P. G. Heath & N. C. Hyatt "Dissolution of UK high-level waste glass under simulated hyperalkaline conditions of a collocated geological disposal facility" *Int. J. Appl. Glass Sci.* **4** (2013) 341-356. DOI: 10.1111/ijag.12042

[18] "Standard test methods for determining chemical durability of nuclear, hazardous, and mixed waste glasses and multiphase glass ceramics: the product consistency test (PCT)" ASTM C1285-02 (2008).

[19] D. L. Parkhurst and C. A. J. Appelo, "Description of input and examples for PHREEQC version 3—A computer program for speciation, batch-reaction, one-dimensional transport, and inverse geochemical calculations: U.S. Geological Survey Techniques and Methods, book 6, chap. A43, 2013.

[20] K. J. D. Mackenzie and M. E. Smith, *Multinuclear Solid-State NMR of Inorganic Materials*, *Pergamon Materials Series Vol 6*. Amsterdam: Pergamon, 2002.

[21] D. J. Backhouse, A. J. Fisher, J. J. Neeway, C. L. Corkhill, N. C. Hyatt and R. J. Hand "Corrosion of the International Simple Glass (ISG) under acidic to hyperalkaline conditions" npj Mater. Degrad. **2** (2018) 29 DOI: 10.1038/s41529-018-0050-5

[22] C. Biagioni, S. Merlino and E. Bonaccorsi, "The tobermorite supergroup: a new nomenclature," *Miner. Mag.* **79** (2015) 485-495

[23] H. Yamashita, H. Yoshino, K. Nagata, H. Inoue, T. Nakajin, and T. Maekawa, "Nuclear magnetic resonance studies of alkaline earth phosphosilicate and aluminoborosilicate glasses," *J. Non. Cryst. Solids*, vol. 270, no. 1, pp. 48–59, 2000.

[24] H. Yamashita, K. Inoue, T. Nakajin, H. Inoue, and T. Maekawa, "Nuclear magnetic resonance studies of 0.139MO (or M'_2O)·0.673SiO_2·(0.188−x)Al_2O_3·xB_2O_3 (M=Mg, Ca, Sr and Ba, M'=Na and K) glasses," *J. Non. Cryst. Solids*, vol. 331, no. 1, pp. 128–136, 2003.

[25] A.J. Connelly, N.C. Hyatt, K.P. Travis, R.J. Hand and E. Maddrell *Predicting the preference for charge compensation in silicate glasses* Phys. Chem. Glasses: Europ. J. Glass Sci. Technol. B **52** 64-67 (2011)

[26] K. L. Geisinger, R. Oestrike, A. Navrotsky, G. L. Turner, and R. J. Kirkpatrick, "Thermochemistry and structure of glasses along the join $NaAlSi_3O_8$-$NaBSi_3O_8$," *Geochim. Cosmochim. Acta*, vol. 52, no. 10, pp. 2405–2414, 1988.

[27] S. K. Lee and J. F. Stebbins, "The Structure of Aluminosilicate Glasses: High-Resolution 17O and

27Al MAS and 3QMAS NMR Study," *J. Phys. Chem. B*, vol. 104, no. 17, pp. 4091–4100, 2000.

[28] W. Loewenstein, "The distribution of aluminum in the tetrahedra of silicates and aluminates" *Amer. Mineral.*, vol. 39, pp. 92–96, 1954.

[29] R. Guo, C. T. Brigden, S. Gin, S. W. Swanton and I. Farnan, "The effect of magnesium on the local structure and initial dissolution rate of simplified UK Magnox waste glasses," *J. Non-Cryst. Solids*, vol. 497, pp 82–92, 2018.

[30] E. M. Pierce, L.R. Reed, *et al.*, "Experimental determination of the effect of the ratio of B/Al on glass dissolution along the nepheline (NaAlSiO4)-malinkoite (NaBSiO4) join," *Geochim. Cosmochim. Acta*, vol. 74, no. 9, pp. 2634–2654, 2010.

[31] I. Techer, T. Advocat, J. Lancelot, and J. M. Liotard, "Basaltic glass: Alteration mechanisms and analogy with nuclear waste glasses," *J. Nucl. Mater.*, **282**, 40–46, 2000.

[32] I. W. Donald, B.L. Metcalfe and R. N. J. Taylor "The immobilization of high level radioactive wastes using ceramics and glasses" *J. Mater. Sci.* **32** (1997) 5851-5887

[33] P. Frugier, C. Martin, I. Ribet, T. Advocat, and S. Gin, "The effect of composition on the leaching of three nuclear waste glasses: R7T7, AVM and VRZ," *J. Nucl. Mater.*, vol. 346, no. 2–3, pp. 194–207, 2005.

[34] E. Curti, J. L. Crovisier, G. Morvan, and A. M. Karpoff, "Long-term corrosion of two nuclear waste reference glasses (MW and SON68): A kinetic and mineral alteration study," *Appl. Geochemistry*, vol. 21, no. 7, pp. 1152–1168, 2006.

[35] M. Debure, P. Frugier, L. De Windt, and S. Gin, "Dolomite effect on borosilicate glass alteration," *Appl. Geochemistry*, vol. 33, pp. 237–251, 2013.

[36] M. Debure, L. De Windt, P. Frugier, and S. Gin, "HLW glass dissolution in the presence of magnesium carbonate: Diffusion cell experiment and coupled modeling of diffusion and geochemical interactions," *J. Nucl. Mater.*, vol. 443, no. 1–3, pp. 507–521, 2013.

[37] M. Debure, L. De Windt, P. Frugier, S. Gin, and P. Vieillard, "Mineralogy and thermodynamic properties of magnesium phyllosilicates formed during the alteration of a simplified nuclear glass," *J. Nucl. Mater.*, vol. 475, pp. 255–265, 2016.